# Modeling Rain-Induced Effects on Boundary-Layer Wind Field of Tropical Cyclones

Reda Snaiki, Teng Wu*

*Department of Civil, Structural and Environmental Engineering, University at Buffalo, Buffalo, NY 14126, USA*

*Corresponding author. Email: tengwu@buffalo.edu

**Abstract:** Despite the significant impacts of heavy rainfall on the tropical cyclone intensity due to the transfer of horizontal momentum between air and raindrops, the comprehensive modeling of rain-induced effects on the boundary-layer wind field remains a challenge. The wind shear zone developed surrounding the falling precipitation results in complicated dynamic interactions between the wind and rain fields. The solution of dynamically coupled, intensively interactive wind and rain fields can be achieved using high-fidelity air-water interaction simulations but needs extremely high computational costs. To consider the wind-rain interactions with a first-order approximation, the fully-coupled dynamic system governing the raindrop motion and the wind field has been simplified herein to a weakly-coupled one represented by aerodynamic drag force. The drag-induced horizontal momentum transfer is integrated into the governing equations of the linear, height-resolving wind field, and an analytical model is accordingly developed to effectively consider the rain-induced effects on the boundary-layer winds of tropical cyclones. The results generated by the present model are consistent with the field measurements. It has been demonstrated that, while the wind speed can be either accelerated or decelerated depending on the location in the tropical cyclones and the rain parameters (e.g., rain rate, relative motion between the air and raindrops, drag coefficient and raindrop size distribution), the rain-induced effects on the boundary-layer wind directions (and hence the inflow angle) also have important significance on the tropical cyclone wind hazard on tall buildings and other of structures. Due to its high

computational efficiency, the proposed model could be easily implemented in the risk assessments for tropical-cyclone wind hazards in engineering applications.

**Keywords:** *Tropical cyclone, boundary layer winds, raindrops, raindrop size distribution, Monte Carlo technique*.

## 1. Introduction

Tropical cyclone-related natural hazards are well known for resulting in the largest contribution to insured losses each year (Landsea 2000; Rappaport 2000). High winds and heavy rainfall in the tropical cyclone boundary layer cause widespread damage to life and property in coastal areas. Consequently, there is much interest in the assessment of the boundary-layer wind (e.g., Meng et al. 1995; Kepert 2001; Snaiki and Wu 2017a, 2017b, 2018a) and rain fields (e.g., Langousis and Veneziano 2009; Snaiki and Wu 2018b). While the wind-induced effects on the rain field has been extensively investigated in the context of wind-driven rain (e.g., Choi 2001; Blocken and Carmeliet 2000a, 2000b, 2004; Huang and Li 2010; Fu et al. 2015), limited studies have considered the rain-induced effects on the wind field. However, Pauluis and Dias (2012) demonstrated that a substantial amount of frictional dissipation in the atmosphere occurs in the microphysical shear zones surrounding falling raindrops, and hence the rain-induced effects on winds cannot be disregarded. Based on the satellite data from the Tropical Rainfall Measurement Missions (TRMM) coupled with a modified version of the Carnot-heat-engine model, Sabuwala et al. (2015) showed that the tropical cyclone intensity could be reduced by almost 20% due to rainfall.

Several experimental studies confirmed an important reduction of the mean wind speed due to the presence of rain. Ho et al. (2007) compared the boundary-layer winds with/without rain at University of Delaware's Air-Sea Interaction Laboratory and found that the mean wind speed profile decreased substantially because of the high rain rates. This observation deviates from the previous studies by Janin and Cermak (1988) and Pielke and Lee (1991) that the atmospheric wind

profiles under the airborne sediment or raindrops remain unchanged. Harrison et al. (2012) further investigated the combined effects of wind and rain on air-water gas exchange with eight different wind speeds and three rain rates, and highlighted that the observed mean wind speed profiles decrease with rain rate. It should be noted that the raindrops in the above-mentioned experimental setup were released from a selected height with zero horizontal velocity, hence they have been accelerated by the wind as they fell. In the tropical cyclone, the momentum exchange between the wind and raindrops can be much more complicated since the wind speed profiles (including a supergradient region) differ from one location to another.

Although it is well known that the rain-induced effects on the wind field is mainly due to the transfer of horizontal momentum, there is no well-established analysis framework that could be used to effectively simulate the wind-rain interactions. Caldwell and Elliott (1972) and Shapiro (2005) established the coupled equations of motion for the air and raindrops by introducing a drag-induced body force associated with relative motion between the falling particle and the air. While Caldwell and Elliot (1972) considered the wind structure in a rainy surface layer, Shapiro (2005) focused the rain-induced effects on winds in the free atmosphere. In addition, both of these two studies assumed the air and raindrops are horizontally homogenous and unidirectional, and hence the rain-induced effects on the boundary-layer wind direction was not considered.

In this study, the drag-induced horizontal momentum transfer is integrated into the governing equations of the linear, height resolving wind field, and an analytical model is accordingly developed to effectively consider the rain-induced effects on the boundary-layer winds of tropical cyclones. More specifically, the wind velocity is expressed as the summation of the gradient wind in the free atmosphere and frictional component near the ground surface. Both of these two components are determined analytically by solving the simplified governing equations that include the rain-induced aerodynamic drag force. The key rain parameters involved in the wind field simulation, such as the rain rate, relative motion between the air and raindrops, drag

coefficient and raindrop size distribution for tropical cyclones have been comprehensively discussed and appropriately selected. The results generated by the developed model to consider rain-induced effects on the boundary-layer winds of tropical cyclones are consistent with field measurements. The wind speed was found to be either accelerated or decelerated depending on the location inside the tropical cyclone and the rain parameters. Furthermore, the simulation results indicated that the rain-induced effects on the boundary-layer wind directions (and hence the inflow angle) also have important significance on the tropical cyclone wind hazard on tall buildings and other structures. The proposed model, due to its high computational efficiency, can be used in conjunction with the Monte Carlo techniques to perform risk analysis of tropical-cyclone wind hazards.

## 2. Governing Equations of Boundary-Layer Winds

Rain has little effects on the statistics of wind fluctuations, as measured using a wind spectrum (Aylor and Ducharme 1995). Hence, the rain-induced effects on the mean wind field are focused here. The fully-coupled dynamic air-water interaction system can be simplified into a weakly-coupled one represented by the mean aerodynamic drag force. In the boundary layer of a tropical cyclone, the horizontal momentum equations are solved with a prescribed pressure distribution and a constant air density. To account for the horizontal force associated with the relative motion between the raindrops and air, the drag force $\boldsymbol{f_d}$ exerted by rain on air is included in the governing equation of the height-resolving wind field of a tropical cyclone:

$$\frac{\partial \boldsymbol{v}}{\partial t} + \boldsymbol{v}.\nabla \boldsymbol{v} = -\frac{1}{\rho_a}\nabla p - f\boldsymbol{k} \times \boldsymbol{v} + \boldsymbol{F} + \frac{1}{\rho_a}\boldsymbol{f}_d \tag{1}$$

where $\boldsymbol{v}$ = wind velocity; $f$ = Coriolis parameter; $\boldsymbol{k}$ = unit vector in the vertical direction; $\boldsymbol{F}$ = frictional force; $\rho_a$ = air density; and $p$ = Holland pressure expressed as (Holland 1980):

97 $$p = p_c + \Delta p \exp\left[-\left(r_m / r\right)^B\right] \quad (2)$$

98 where $p_c$ = central pressure; $\Delta p$ = central pressure difference; and $B$ = Holland's radial pressure
99 parameter. To solve Eq. (1), the decomposition method is used in which the wind velocity is
100 decomposed into gradient wind $\boldsymbol{v_g}$ and frictional wind $\boldsymbol{v'}$ (Meng et al. 1995; Kepert 2001; Snaiki
101 and Wu 2017a, 2017b):

102 $$\boldsymbol{v} = \boldsymbol{v_g} + \boldsymbol{v'} \quad (3)$$

103 Consequently two separate equations can be derived:

104 $$\frac{\partial \boldsymbol{v_g}}{\partial t} + \boldsymbol{v_g}.\nabla \boldsymbol{v_g} = -\frac{1}{\rho_a}\nabla p - f\boldsymbol{k} \times \boldsymbol{v_g} + \boldsymbol{f}_{d,g} \quad (4a)$$

105 $$\frac{\partial \boldsymbol{v'}}{\partial t} + \boldsymbol{v'}.\nabla \boldsymbol{v'} + \boldsymbol{v'}.\nabla \boldsymbol{v_g} + \boldsymbol{v_g}.\nabla \boldsymbol{v'} = -f\boldsymbol{k} \times \boldsymbol{v'} + \boldsymbol{F} + \boldsymbol{f}_{d,s} \quad (4b)$$

106 where $\boldsymbol{f}_{d,g}$ = drag force exerted by rain on air at the gradient level; and $\boldsymbol{f}_{d,s}$ = drag force exerted
107 by rain on air corresponding to the frictional wind speed. Equations (4a) and (4b) are further
108 simplified by assuming that the gradient wind pattern $\boldsymbol{v_g}$ is moving in the free atmosphere at the
109 translation velocity of the tropical cyclone $\boldsymbol{c}$, thus the unsteady term can be expressed as:
110 $\frac{\partial \boldsymbol{v_g}}{\partial t} = -\boldsymbol{c}.\nabla \boldsymbol{v_g}$. On the other hand, the unsteady term $\frac{\partial \boldsymbol{v'}}{\partial t}$ is significantly smaller than the turbulent
111 viscosity and inertia terms in the tropical cyclone boundary layer, and hence neglected (Meng et
112 al. 1995).

113 To determine the drag force $\boldsymbol{f_d}$, first the drag force $\boldsymbol{f}_i$ exerted by one raindrop on air in the
114 horizontal direction is introduced [Fig. 1]. Based on a photographic study, Okaruma and Nakanishi
115 (1969) concluded that the raindrops deformation is random and suggested that a spherical shape
116 of the raindrops could be reasonably assumed (e.g., Caldwell and Elliot 1971, 1972; Shapiro 2005).

117 Accordingly, the drag force $\boldsymbol{f}_i$ exerted by one raindrop on air in the horizontal direction is
118 expressed as:

119 $$\boldsymbol{f}_i = \frac{1}{8}\rho_a C_r V_{rel}(\boldsymbol{V}_{rain} - \boldsymbol{V}_{wind})\pi d^2 \quad (5)$$

120 where $C_r$ = drag coefficient for a raindrop of diameter $d$; $\boldsymbol{V}_{rain}$ = raindrop horizontal velocity; $\boldsymbol{V}_{wind}$
121 = wind velocity in the horizontal direction; and $V_{rel}$ = the total relative speed of the raindrop that
122 can be expressed as:

123 $$V_{rel} = \sqrt{w^2 + (v_{\theta,wind} - v_{\theta,rain})^2 + (v_{r,wind} - v_{r,rain})^2} \quad (6)$$

124 where $v_{\theta,wind}$ = azimuthal component of the wind velocity; $v_{r,wind}$ = radial component of the wind
125 velocity; $v_{\theta,rain}$ = azimuthal component of the raindrop velocity; $v_{r,rain}$ = radial component of the
126 raindrop velocity; and $w$ = vertical raindrop velocity component assumed to be equal to the
127 terminal velocity $w_t$ in the boundary-layer region of a tropical cyclone (Shapiro 2005, Pauluis and
128 Dias 2012). The relative velocity can be approximated as $V_{rel} \approx |w_t|$ considering
129 $|w_t| \gg |v_{\theta,wind} - v_{\theta,rain}|$ and $|w_t| \gg |v_{r,wind} - v_{r,rain}|$ (Poreh and Mechrez 1984; Shapiro 2005).

130
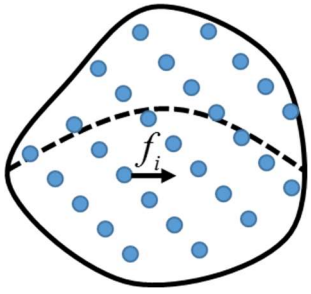


131 **Fig. 1.** Drag force exerted by raindrops on air

132 The total drag force $\boldsymbol{f}_d$ applied on a tiny volume of air, in which a uniform raindrop size
133 can be assumed, is then expressed in the form $n\boldsymbol{f}_i = NV\boldsymbol{f}_i / |w_t|$ where $n$ denotes the total number of

raindrops in the volume $V$ and $N$ is the number of raindrops per second on a unit area. The parameter $N$ is assessed in terms of the rain rate $R$ based on the spherical shape assumption as $N = \frac{6R}{\pi d^3}$. Accordingly, the total drag force in Eq. (1) can be expressed as:

$$\boldsymbol{f_d} = \frac{3R\rho_a C_r(\boldsymbol{V_{rain}} - \boldsymbol{V_{wind}})}{4d} \tag{7}$$

where the raindrops horizontal velocity and their corresponding wind velocity is empirically correlated as $\boldsymbol{V}_{rain} - \boldsymbol{V}_{wind} = -\gamma \boldsymbol{V}_{wind}$ and the correlation parameter $\gamma$ can be experimentally or numerically identified.

## 3. Decomposition Approach

In this section the gradient wind velocity of a stationary tropical cyclone will be first provided, then the solution of a moving tropical cyclone will be obtained by modifying the governing equations of the stationary case based on the Blaton's formula. The frictional wind components will be also determined using a linear, height-resolving solution.

### 3.1 Gradient wind velocity

#### 3.1.1 Stationary tropical cyclone

The two components of the gradient wind velocity $v_{rg}$ and $v_{\theta g}$ can be determined using the cylindrical coordinates system $(r, \theta, z)$. Accordingly, the Eq. (4a) can be expressed as:

$$v_{rg}\frac{\partial v_{rg}}{\partial r} - \frac{{v_{\theta g}}^2}{r} = -\frac{1}{\rho_a}\frac{\partial p}{\partial r} + f v_{\theta g} - A v_{rg} \tag{8a}$$

$$v_{rg}\frac{\partial v_{\theta g}}{\partial r} + \frac{v_{\theta g} v_{rg}}{r} = -f v_{rg} - A v_{\theta g} \tag{8b}$$

where $A = \frac{3C_r R}{4d}\gamma$ . The gradient wind components can be determined based on Eq. (8a) and (8b) along with the continuity equation. After some mathematical manipulations, a new set of equations governing the azimuthal and radial components of the gradient wind are obtained as follows:

$$\left(1+\frac{A^2}{\xi_{ag}{}^2}\right)\frac{v_{\theta g}{}^2}{r}+\left(f+\frac{A^2}{\xi_{ag}{}^2}\right)v_{\theta g}-\frac{1}{\rho_a}\frac{\partial p}{\partial r}=0 \tag{9a}$$

$$v_{rg} = -\frac{A}{\xi_{ag}}v_{\theta g} \tag{9b}$$

where $\xi_{ag} = \frac{\partial v_{\theta g}}{\partial r}+\frac{v_{\theta g}}{r}+f$ is the vertical component of absolute vorticity of the gradient wind (e.g., Vogl and Smith 2009). The iteration process is necessary to determine the gradient wind speed components since $v_{\theta g}$ and $\xi_{ag}$ depend on each other. On the other hand, it is noted that the rain-induced effects on $\xi_{ag}$ is negligible. Therefore, $\xi_{ag}$ is computed herein based on the available formula for the stationary tropical cyclones (Georgiou 1986). Solving Eq. (9a) leads to the following formula of $v_{\theta g}$ :

$$v_{\theta g} = \frac{-\left(f+\frac{A^2}{\xi_{ag}}\right)+\left[\left(f+\frac{A^2}{\xi_{ag}}\right)^2+\frac{4}{\rho_a r}\frac{\partial p}{\partial r}\left(1+\frac{A^2}{\xi_{ag}{}^2}\right)\right]^{1/2}}{\frac{2}{r}\left(1+\frac{A^2}{\xi_{ag}{}^2}\right)} \tag{10}$$

### 3.1.2 Moving tropical cyclone

Based on the field measurements, it has been reported that the spatial asymmetry of the gradient wind speed between the tropical cyclone right and left sides could be well captured using the Blaton's formula (Georgiou 1986). Hence, the Blaton's formula is utilized to solve for the gradient wind speed for a moving tropical cyclone, where the tropical cyclone radius is replaced by

169 $r\Big/\left[1-\frac{c}{v_{\theta g}}\sin(\beta-\theta)\right]$ (Georgiou 1986). Accordingly, the governing equation of the gradient

170 wind component for a moving tropical cyclone becomes:

171 $$\left(1+\frac{A^2}{\xi_{ag}{}^2}\right)\frac{v_{\theta g}{}^2}{r}+\left[f+\frac{A^2}{\xi_{ag}{}^2}-\frac{c\sin(\beta-\theta)}{r}\left(1+\frac{A^2}{\xi_{ag}{}^2}\right)\right]v_{\theta g}-\frac{1}{\rho_a}\frac{\partial p}{\partial r}=0 \tag{11}$$

172 As a result, the tangential gradient wind speed is determined by the following formula:

173 $$v_{\theta g}=\frac{-\left(f+\frac{A^2}{\xi_{ag}}\right)+\frac{c\sin(\beta-\theta)}{r}\left(1+\frac{A^2}{\xi_{ag}{}^2}\right)}{\frac{2}{r}\left(1+\frac{A^2}{\xi_{ag}{}^2}\right)}+\frac{\left[\left(f+\frac{A^2}{\xi_{ag}}-\frac{c\sin(\beta-\theta)}{r}\left(1+\frac{A^2}{\xi_{ag}{}^2}\right)\right)^2+\frac{4}{\rho_a r}\frac{\partial p}{\partial r}\left(1+\frac{A^2}{\xi_{ag}{}^2}\right)\right]^{1/2}}{\frac{2}{r}\left(1+\frac{A^2}{\xi_{ag}{}^2}\right)} \tag{12}$$

174 Equation (12) reduces to the well-known formula $v_{\theta g}=\frac{\left(-csin(\theta-\beta)-fr\right)}{2}+\left[\frac{\left(-csin(\theta-\beta)-fr\right)^2}{4}+\frac{r}{\rho}\frac{\partial p}{\partial r}\right]^{1/2}$

175 without consideration of the rain effects on the wind speed (e.g., Georgiou 1986; Meng et al. 1995).

176 **3.2 Frictional wind velocity**

177 As in Meng et al. (1995) and Snaiki and Wu (2017a, 2017b) the nonlinear Eq. (4b) could be
178 simplified using the scale analysis, and then linearized. Accordingly, the friction wind components
179 considering the rain effects can be determined using the following linear, height-resolving
180 equations:

181 $$-\left(2\frac{v_{\theta g}}{r}+f\right)v'_\theta=k\frac{\partial^2 v'_r}{\partial z^2}-\frac{3C_r R}{4d}\gamma v'_r \tag{13a}$$

$$\left(\frac{\partial v_{\theta g}}{\partial r}+\frac{v_{\theta g}}{r}+f\right)v_r'=k\frac{\partial^2 v_\theta'}{\partial z^2}-\frac{3C_rR}{4d}\gamma v_\theta' \tag{13b}$$

where $k$ = eddy viscosity. Introducing the absolute angular velocity $\xi_g=2\frac{v_{\theta g}}{r}+f$, $p=\frac{1}{2k}\xi_g$ and $q=\frac{1}{2k}\xi_{ag}$, Eqs. (13a) and (13b) can be simplified as:

$$-2pv_\theta'=\frac{\partial^2 v_r'}{\partial z^2}-\frac{A}{k}v_r' \tag{14a}$$

$$2qv_r'=\frac{\partial^2 v_\theta'}{\partial z^2}-\frac{A}{k}v_\theta' \tag{14b}$$

To more conveniently solve Eqs. (14a) and (14b), an additional variable $\omega=\sqrt{\frac{q}{p}}v_r'+iv_\theta'$ is introduced leading to the following equation:

$$\frac{\partial^2\omega}{\partial z^2}-\left(\frac{A}{k}+2i\sqrt{pq}\right)\omega=0 \tag{15}$$

Setting $a=\sqrt{\frac{A/k+\sqrt{A^2/k^2+4pq}}{2}}$ and $b=\sqrt{\frac{\sqrt{A^2/k^2+4pq}-A/k}{2}}$, Eq. (15) can be written in the following format:

$$\frac{\partial^2\omega}{\partial z^2}-(a+ib)^2\omega=0 \tag{16}$$

The perturbations $v_r'$ and $v_\theta'$ must go to zero at very high altitudes, where the solution of Eq. (16) becomes $\omega=(W_1+iW_2)\exp\left[-(a+ib)z'\right]$. Accordingly, the frictional wind speed components can be determined as:

$$v_r'=Ye^{-az'}\left[W_1\cos(bz')+W_2\sin(bz')\right] \tag{17a}$$

197 $$v'_\theta = e^{-az'}\left[W_2\cos(bz') - W_1\sin(bz')\right] \quad (17b)$$

198 where $Y = \sqrt{p/q}$ . The coefficients $W_1$ and $W_2$ can be obtained as follows:

199 $$W_1 = -\frac{\left(a/b + \chi - T\right)\left(\chi/Y - T/Y\right)v_{rg} + (\chi - T)v_{\theta g}}{1 + \left(\frac{a}{b} + \chi - T\right)^2} \quad (18a)$$

200 $$W_2 = \frac{\left(\chi/Y - T/Y\right)v_{rg} - \left(a/b + \chi - T\right)(\chi - T)v_{\theta g}}{1 + \left(a/b + \chi - T\right)^2} \quad (18b)$$

201 where $\chi = \frac{C_a|v_s|}{kb}$; $T = \frac{\gamma_r \rho_d R}{\rho_a bk}$; and $\boldsymbol{v_s}$ = total wind velocity near the ground surface. To solve for

202 the solutions of $v'_r$ and $v'_\theta$, the boundary conditions at the upper atmosphere $\left(\boldsymbol{v'}|_{z'\to\infty} = 0\right)$ and near

203 the surface (using the bulk formulation with drag coefficient $C_a$) have been utilized in this study

204 (e.g., Kepert 2001). It should be stressed out that the raindrops produce both vertical and horizontal

205 stresses on the surface ( $\boldsymbol{\tau}_r = \gamma_r \rho_d \boldsymbol{V}_{wind} R$ ). The frictional velocity model introduced by Meng et al.

206 (1995) and Snaiki and Wu (2017a) is a special solution of Eqs. (17a) and (17b) without considering

207 the rain-induced effects on winds.

208 **4. Rain Parameter Selection**

209 The rain parameters, namely rain rate $R$, correlation parameter $\gamma$, raindrop drag coefficient $C_r$

210 and raindrop size *d* are necessary to consider the rain-induced effects on the boundary-layer winds

211 for a given tropical cyclone.

212 **4.1 Rain rate *R***

213 A number of field measurements and numerical simulations indicate that the rain rate increases

214 from the storm center towards the radius of maximum winds, then decays exponentially far away

from the center (e.g., Lonfat et al., 2004; Tuleya et al., 2007; Langousis and Veneziano, 2009; Snaiki and Wu 2018b). Accordingly, a simplified parametric formula for the rain rate is proposed here in the case of marine condition as follows:

$$R = R_{rm}\left\{\left(\frac{r_m}{r}\right)^{b'} \exp\left[1-\left(\frac{r_m}{r}\right)^{b'}\right]\right\}^{0.5} \tag{19}$$

where $R_{rm}$ = maximum rain rate located at the radius of maximum wind $r_m$; $r$ = radial distance from the tropical cyclone center; and $b'$ = scaling parameter that adjusts the profile shape and depends on the radial extent of the tropical cyclone rain field. The maximum rain rate $R_{rm}$ is estimated based on an empirical formula introduced by Tuleya et al. (2007):

$$R_{rm} = a^* + b^*\left[1+\left(V_m - 18.0056\right)/16.9767\right] \tag{20}$$

where $a^*$ and $b^*$ = constants from the least squares fit of the TRMM radial rainfall rates; and $V_m$ = maximum wind speed in *m/s*. Hurricane Gordon (2006) that reached category 3 on the Saffir-Simpson scale was selected to validate the proposed empirical rain rate model. Figure 2 depicts the simulated ($b' = 4$) and observed radial profiles, and the simulation results match well with the observations. The choice of an appropriate value of $b'$ could be empirically derived (e.g., Tuleya et al. 2007).

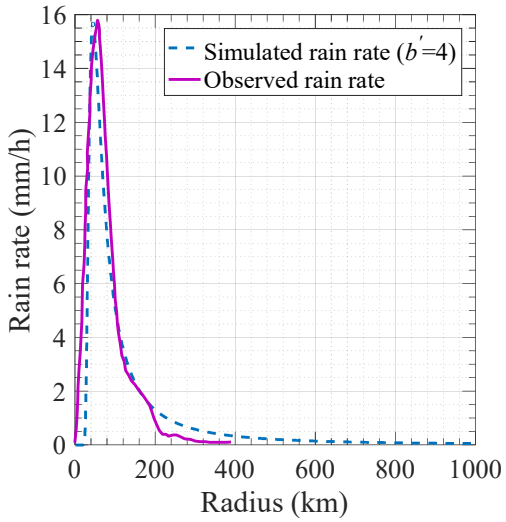


**Fig. 2.** Comparison of azimuthally averaged rain rates of Hurricane Gordon

For landfalling situations where the rain rate in the eye region might be important, a more elaborate rain rate profile inspired from the wind profile of Willoughby et al. (2006) is proposed and consists of three piecewise continuous functions patched smoothly together:

$$R(r) = R_1 = R_0 + \left(R_{rm} - R_0\right)\left(\frac{r}{r_m}\right)^n \qquad \left(0 \le r \le r_1\right) \tag{21a}$$

$$R(r) = R_1\left(1-w\right) + R_2 w \qquad \left(r_1 \le r \le r_2\right) \tag{21b}$$

$$R(r) = R_2 = R_{rm}\exp\left(-\frac{r-r_m}{r_x}\right) \qquad \left(r_2 \le r\right) \tag{21c}$$

where $n$ = exponent for the power law [i.e., Eq. 21(a)] inside the eye region; $R_0$ = rain rate at the tropical cyclone center determined empirically as $R_0 = c^* + d^*\left[1 + \left(V_m - 18.0056\right)/16.9767\right]$ (Tuleya et al. 2007); and $w$= weighting function that increases monotonically from 0 to 1 in the zone $r_1 \le r \le r_2$. While Eqs. (21a) and (22c) represent the eye and outer rain intensity profiles, respectively, Eq. (21b) can be regarded as the transition function. The empirical Rankine-like profile developed by Tuleya et al. (2007) can be regarded as a special case of the proposed model denoted by [Eqs. (21a), (21b), and (21c)] where the transition zone and exponent $n$ are set equal

to 0 and 1, respectively. The location of the transition zone is obtained by setting the radial derivative of Eq. (21b) to be equal to 0 at $r = r_m$ (Willoughby et al. 2006). It should be pointed out that the Eq. (21c) can be replaced by a dual exponential profile (Willoughby et al. 2006) to capture different decay rates of the rain intensity outside the eyewall. Figure 3 depicts the comparison between the simulated rain rate profile and the TRMM-based radial distribution of azimuthally averaged rain rates for hurricane intensity categories 1-2 (CAT12) with winds from 34-48 $m.s^{-1}$ and categories 3-5 (CAT35) with winds > 49 $m.s^{-1}$ (Lonfat et al. 2004; Tuleya et al. 2007). Good agreement between the simulated and observed profiles is achieved.

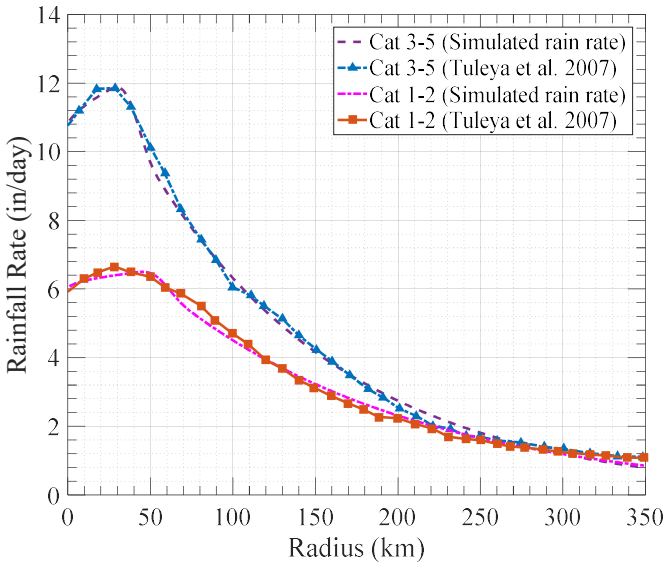


**Fig. 3.** Comparison between simulated and TRMM-based radial profiles of rain rates

### 4.2 Correlation parameter $\gamma$

As highlighted in Sect. 2, the correlation parameter $\gamma$ is utilized to relate the raindrop horizontal velocity and its corresponding wind velocity such that $\boldsymbol{V}_{rain} - \boldsymbol{V}_{wind} = -\gamma \boldsymbol{V}_{wind}$. Guo et al. (2001) proposed an empirical formula $\boldsymbol{V}_{rain} = \psi \boldsymbol{V}_{wind}$, where the horizontal velocity ratio $\psi = 1 \Big/ \left(1 + \sqrt{0.5 C_r}\right)$. This simplified formula actually suggests that the horizontal wind velocity is higher than its corresponding horizontal rain velocity (Liggett 1994; Guo et al. 2001), and hence

might be valid only at higher altitudes where the wind speed increases downward before reaching the supergradient region (see Fig. 4). At the lower altitudes, it has been demonstrated that the horizontal velocity of raindrop (due to its inertia) can be larger than the corresponding wind velocity (Choi 2001; Fu et al. 2015). Hence, the horizontal velocity ratio $\psi = \left(0.2373H^{-0.5008} - 0.0167\right)\left(\frac{d}{3}\right)^{0.8}\left(\frac{\alpha'}{0.12}\right)+1$ (where $\alpha'$ is the power-law exponent and $H$ is the altitude in meter) developed by Fu et al. (2015) is utilized in this study.

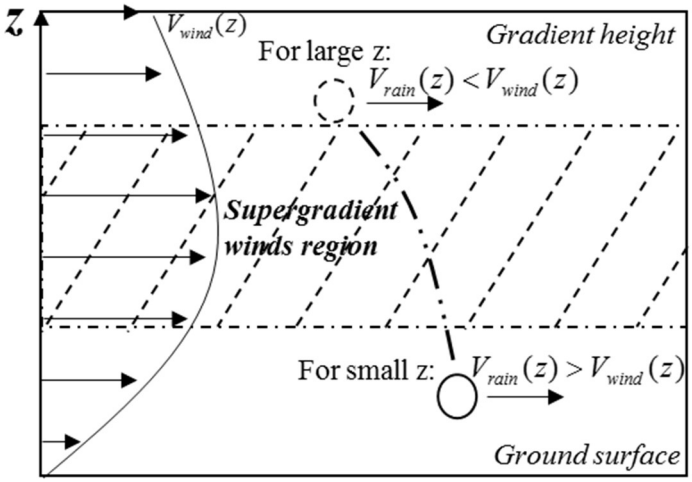


**Fig. 4.** Schematic of droplet velocity relative to wind in the eyewall region

### 4.3 Drag coefficient $C_r$

The drag coefficient $C_r$ of a spherical raindrop is sensitive to the Reynolds number (e.g., Caldwell and Elliot 1971, 1972; Blocken and Carmeliet 2004; Shapiro 2005). Gunn and Kinzer (1949) experimentally identified the values of the drag coefficient and tabulated them as a function of the equivalent raindrop diameter and their corresponding Reynolds numbers. Typical drag coefficient values of the raindrops during tropical cyclones range between 0.45 and 1.05 corresponding to Reynolds numbers between $10^5$ and $10^2$ (e.g., Baheru 2014). Since the raindrops in the tropical cyclones deviate from the spherical shape (Blocken and Carmeliet 2004; Lopez 2011), a sensitivity analysis of the boundary-layer winds to the drag coefficient $C_r$ will be conducted in Sect. 5.

278 **4.4 Raindrop size *d***

279 The raindrop size distribution (RSD) in tropical cyclones have been measured in a number of
280 studies, and various RSD models were accordingly developed (e.g., Marshall and Palmer 1948;
281 Best 1950; Ulbrich 1983; Willis and Tattelman 1989; Tokay 2008). Among them, the three-
282 parameter gamma model has been extensively used since it can depict the observed raindrop
283 spectra with good accuracy (Tokay and Short 1996). The gamma distribution depends on several
284 essential parameters, namely the liquid-water content per unit volume of air $W$, mass-weighted
285 mean diameter $d_{mass}$, characteristic number concentration $N_w$ and shape parameter $m$.
286 Accordingly, the normalized gamma model can be expressed as follows:

287 $$\frac{N(d)}{N_w} = f(m)\left(\frac{d}{d_{mass}}\right)^m \exp\left(-(4+m)\frac{d}{d_{mass}}\right) \tag{22}$$

288 where $N(d)/N_w$ = normalized RSD; $N_w = \frac{4^4}{\pi\rho_d}\left(\frac{W}{d_{mass}^4}\right)$; $f(m) = \frac{6}{4^4}\frac{(4+m)^{m+4}}{\Gamma(m+4)}$ ; and $\Gamma$ = gamma

289 function. The detailed derivation of the mathematical model of the tropical cyclone RSD can be
290 found in Willis (1984), Testud et al. (2001) and Baheru (2014). In this study, the RSD parameters
291 are acquired from Baheru et al. (2014) and Baheru (2014) where the combined datasets from
292 hurricanes Alex, Charley and Gaston (2004) were used. Once the RSD is determined, the raindrop
293 sizes can be generated using the Monte Carlo technique. An example of the wind field simulations
294 based on the raindrop sizes sampled from the RSD is illustrated in Fig. 5, where the mean ($\mu$) of
295 the gradient and frictional wind speeds are plotted along with $\mu+\sigma$ and $\mu-\sigma$ ($\sigma$ denoting the
296 standard deviation of each component).

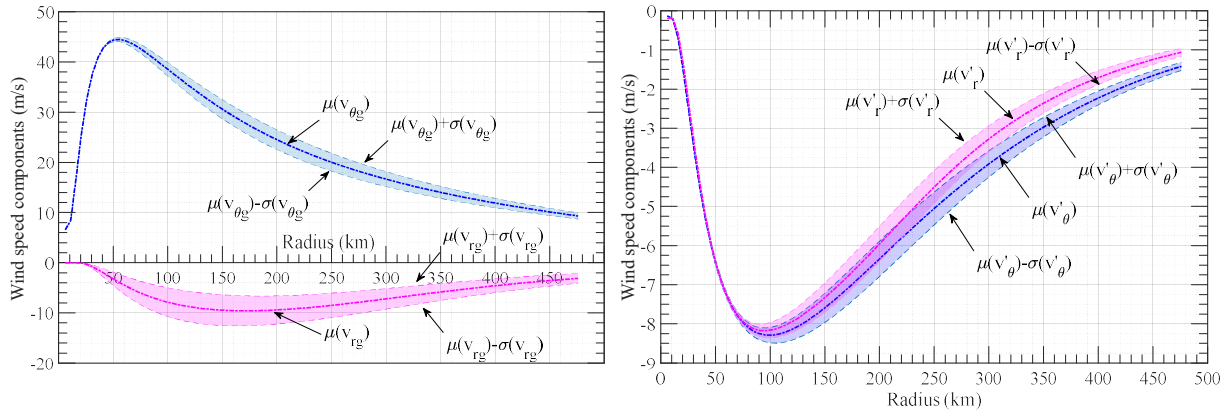


**Fig. 5.** Wind field simulations with random raindrops sizes

## 5. Simulation and Discussion

Once the rain parameters, namely $R$, $\gamma$, $C_r$, and $d$ have been determined along with the storm parameters (approach angle $\beta$, translation velocity $c$, central pressure $p_c$, central pressure difference $\Delta p$, radius of maximum winds $r_m$, Holland's parameter $B$, surface roughness $z_0$, latitude $\psi'$ and longitude $\lambda'$), they could be used as the necessary inputs in the modeling of rain-induced effects on the tropical cyclone wind field as shown in Fig. 6.

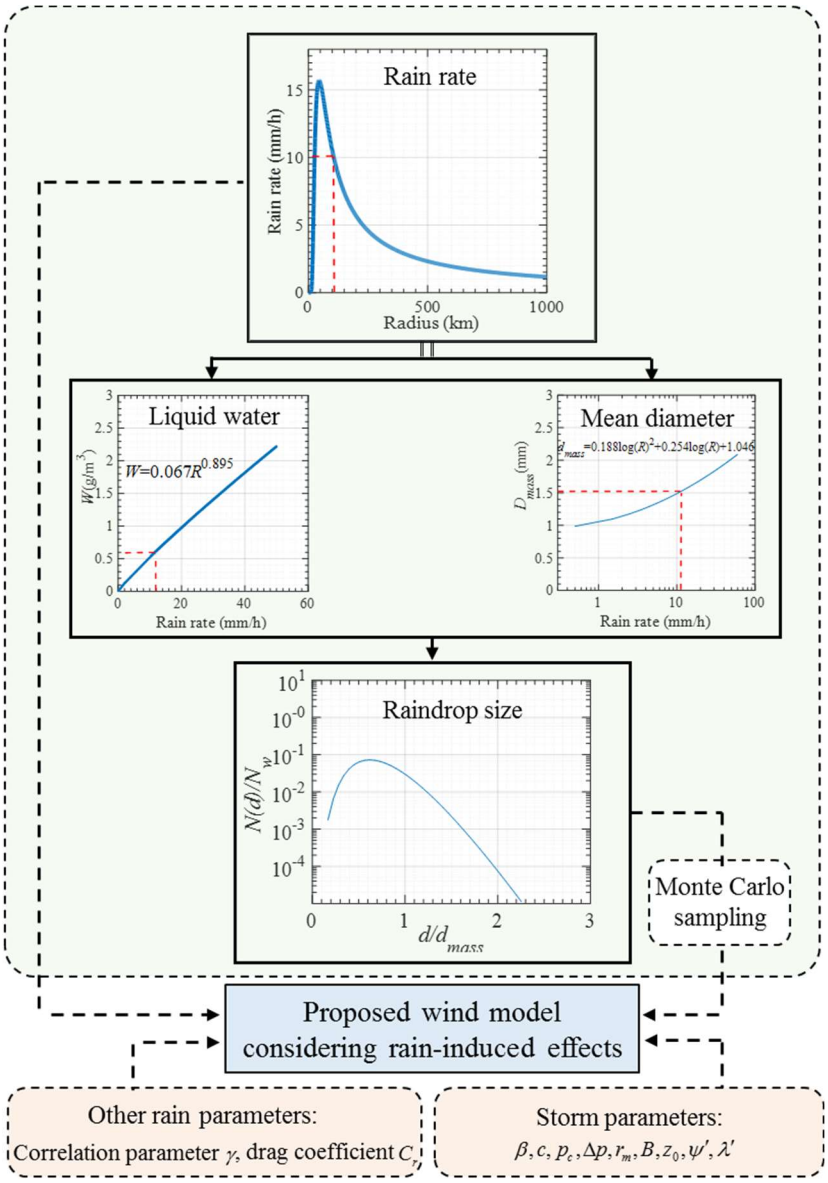


**Fig. 6.** Flowchart of modeling rain-induced effects on tropical cyclone wind field

## 5.1 Comparison with field measurements

Table 1 presents the simulated radial and azimuthal wind components $u$ and $v$, with and without consideration of rain-induced effects denoted by subscripts '$s$' and '$t$', respectively, at three locations [Fig. 7] of Hurricane Sandy (2012) together with their corresponding observations provided by GPS dropsondes (denoted by subscript '$d$'). It should be noted that the dropsondes only provide the instantaneous wind speed profiles, therefore, the comparison is made at the height of 1000 m where the frictional wind components are found negligible. The necessary parameters

needed for the simulation are taken from the National Hurricane Center's North Atlantic Hurricane Database (HURDAT) (Jarvinen et al. 1984).

**Table 1.** Comparison between simulated and measured wind speed for hurricane Sandy (2012)

| Dropsondes ID | $u_d(m/s)$ | $v_d(m/s)$ | $\alpha_d(°)$ | $u_s(m/s)$ | $v_s(m/s)$ | $\alpha_s(°)$ | $u_t(m/s)$ | $v_t(m/s)$ | $\alpha_t(°)$ |
|---|---|---|---|---|---|---|---|---|---|
| 112325032 | -6.2 | 25.7 | 13.5 | -5.7 | 30.2 | 10.7 | -1.9 | 32.0 | 3.5 |
| 112115116 | -5.4 | 19.1 | 15.7 | -4.2 | 21.6 | 10.4 | -3.2 | 22.6 | 3.6 |
| 112115387 | -3.3 | 31.1 | 6.1 | -3.5 | 30.1 | 6.9 | -2.1 | 31.2 | 3.9 |

As shown in Table 1, the radial component of the wind velocity is not negligible as opposed to the common assumption by a number of studies (e.g., Meng et al. 1995; Kepert 2001; Snaiki and Wu 2017a). Hence, the deflection angle (or the inflow angle) $\alpha$ between the wind velocity vector and the tangential unit vector is not equal to zero as usually assumed for the gradient wind (Fig. 7). The obtained logarithmic spiral trajectory based on the simulation results with consideration of rain-induced effects is in accordance with the finding of a number of the field measurements (e.g., Myers and Malkin 1961; Jakobsen and Madsen 2004; Yurchak 2007; Niu et al. 2016). The effects of rain field on the inflow angle within the tropical cyclone boundary layer at various azimuthal and radial locations were further investigated, as in Fig. 8. The simulation results indicate that the rain-induced effects on the boundary-layer directions (and hence the inflow angle) can be important especially within the eyewall region.

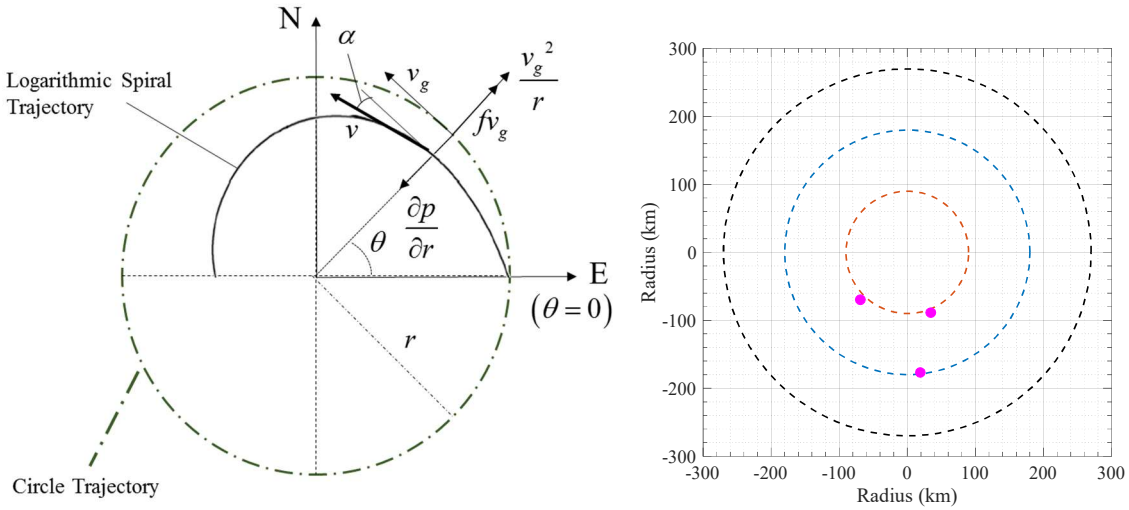


**Fig. 7.** Logarithmic spiral trajectory of the wind particle at gradient wind level (left) and location of selected dropsondes (right)

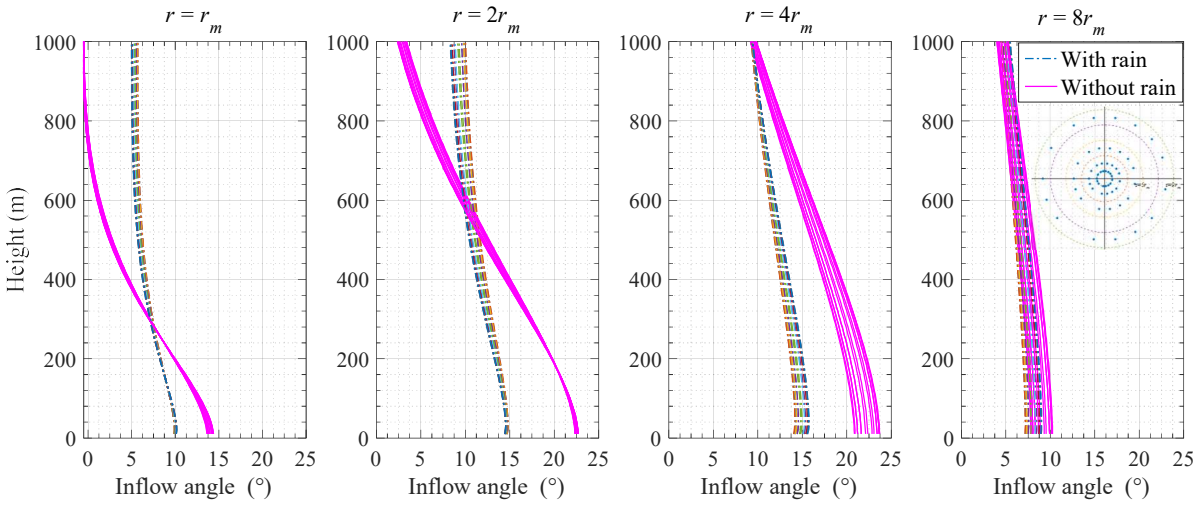


**Fig. 8.** Inflow angle along the height at selected locations

In addition, Hurricane Irma (2017) was selected to validate the simulated surface winds. The estimated maximum intensity reached by Irma was about 80 m/s with a corresponding minimum central pressure of 914 hpa on September 6$^{th}$ 0600 UTC. The anemometer is located on station LTBV3-9751401 (17°41'41" N, 64°45'14" W). As shown in Fig. 9, the results generated by the present wind field model are consistent with hurricane Irma observations.

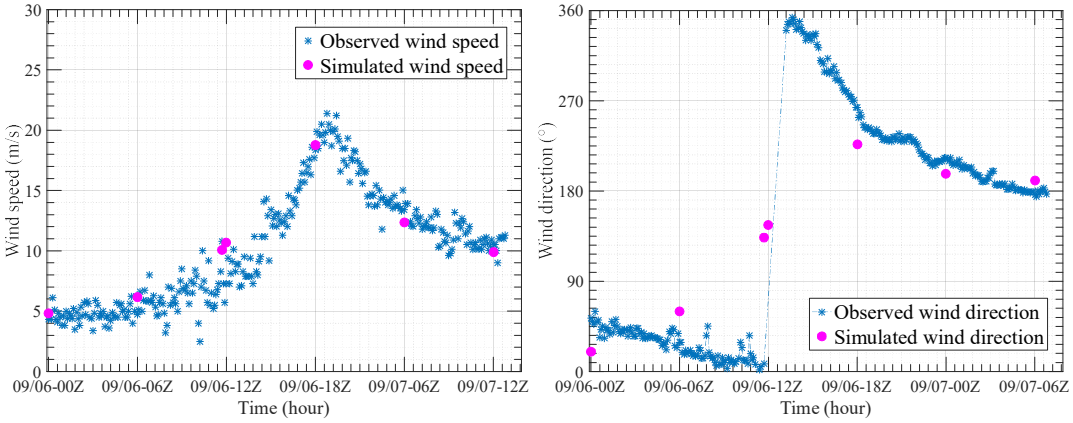


**Fig. 9.** Observed and simulated wind speeds (left) and directions (right) of Hurricane Irma

## 5.2 Simulation results

As discussed in previous sections, the rain-induced effects on the boundary-layer winds of tropical cyclones essentially depend on several rain parameters such as the rain rate $R$ (a function of the maximum rain rate $R_{rm}$ and scaling parameter $b'$), correlation parameter $\gamma$, raindrop drag coefficient $C_r$ and raindrop size $d$. Hence, the sensitivity analyses of the wind field to these rain parameters will be carried out based on the simulation results.

### 5.2.1 Gradient wind

The gradient wind speed components $v_{\theta g}$ and $v_{rg}$ can be calculated using Eqs. (12) and (9b), respectively. Figure 10 represents the sensitivity analysis of the gradient wind speed to the rain parameters of $R_{rm}$, $b'$, $\gamma$, and $C_r$, where a reasonable variation range of the selected parameters was used based on the technical literature (e.g., Gun and Kinzer 1949; Choi 2001; Guo et al. 2001; Shapiro 2005; Baheru 2014; Fu et al. 2015). The necessary storm parameters for the wind field simulation are as follows: $p_c = 960\,hpa$, $B = 1.2$, $c = 7\,m/s$, $\beta = 90°$ and $r_m = 60\,km$, and the baseline rain scenario is taken as: $R_{rm} = 20\,mm/h$, $b' = 2$, $\gamma = 0.1$, $C_r = 0.65$, and $d = 1.6\,mm$. It should be noted that the sensitive analysis of the boundary-layer winds to the raindrop size $d$ has

been presented in Fig. 5, and hence a mean value of the raindrop diameters generated from the selected RSD was employed here for the sake of brevity.

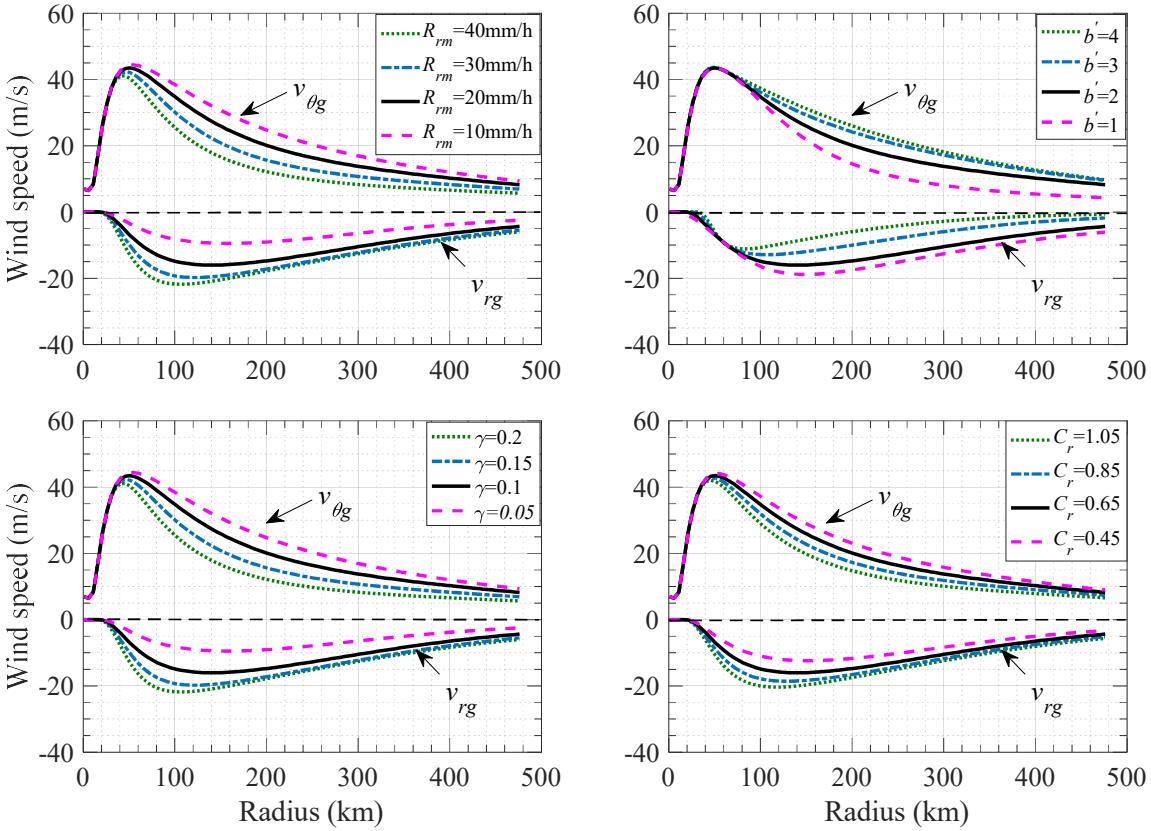


**Fig. 10.** Sensitivity analysis of gradient wind components $v_{\theta g}$ and $v_{rg}$ at height of 1000m with $\theta = 0°$

As shown in Fig. 10, the azimuthal component of the gradient wind speed is mainly influenced by the maximum rain rate $R_{rm}$, scaling parameter $b'$, and correlation parameter $\gamma$. More specifically, $v_{\theta g}$ decreases with $R_{rm}$ and $\gamma$ while increases with $b'$. It is expected that the lower value of $b'$ corresponds to a larger radial extent of the rainfall field and hence more damping effects on the gradient wind speeds. The raindrop drag coefficient $C_r$ has relatively smaller effects on $v_{\theta g}$ compared to other rain parameters. In addition, the radial component of the gradient wind is not negligible and increases with $R_{rm}$ and $\gamma$.

### 5.2.2 Frictional wind

The frictional wind speed components $v'_r$ and $v'_\theta$ can be determined based on Eqs. (17a), (17b), (18a) and (18b). Figure 11 represents the sensitivity analysis of the frictional wind speed to the rain parameters of $R_{rm}$, $b'$, $\gamma_1$ and $C_r$. The necessary storm parameters for the wind field simulations are the same as in Fig. 10 with the additional parameters surface roughness $z_0 = 0.001m$ and eddy viscosity $k = 100 m/s^2$. The baseline rain scenario is taken as: $R_{rm} = 20 mm/h$, $b' = 2$, $\gamma = -0.1$, $C_r = 0.65$ m and $d = 1.6 mm$.

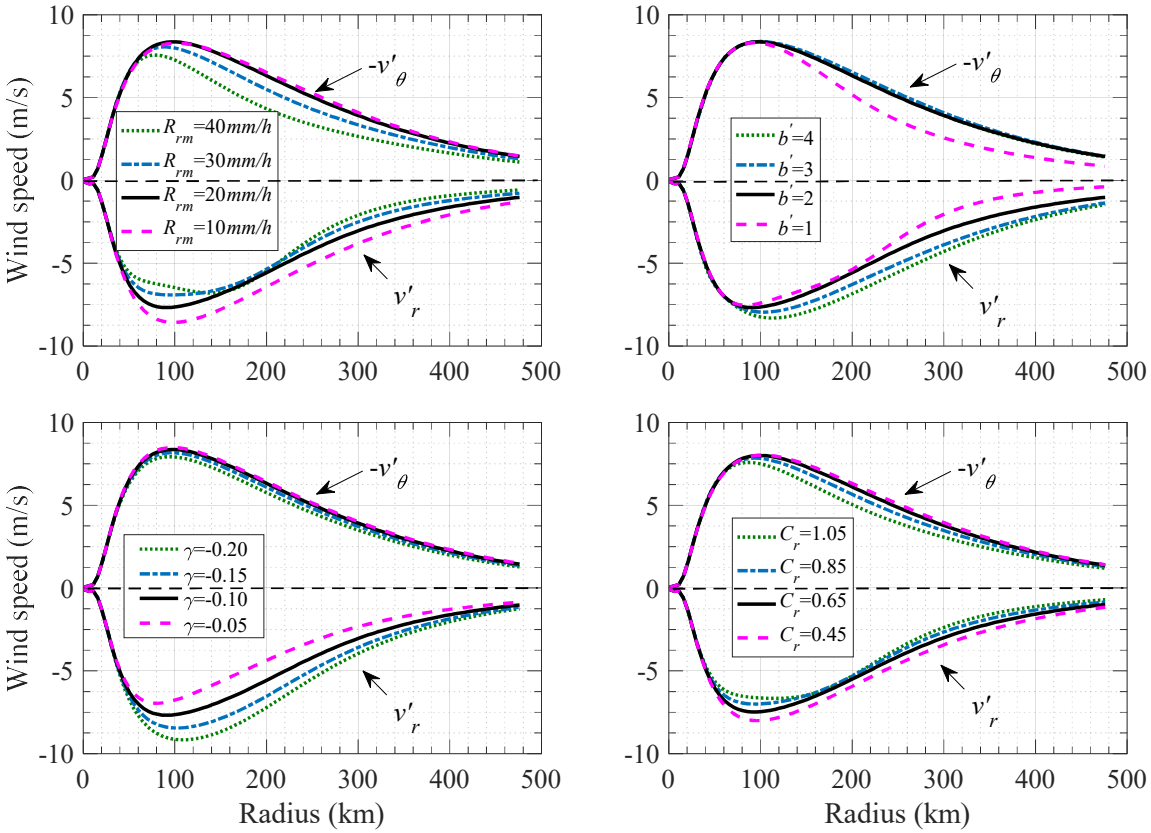


**Fig. 11.** Sensitivity analysis of frictional wind components $v'_r$ and $v'_\theta$ at height of 10m with $\theta = 0°$

As shown in Fig. 10, the higher values of $R_{rm}$ and lower values of $b'$ and $\gamma$ generate lower values of the azimuthal frictional component $v'_\theta$. The radial frictional component $v'_r$ has a similar behavior

as $v'_\theta$ with respect to $R_{rm}$ and $b'$. Furthermore, it is noted that the raindrop drag coefficient $C_r$ also has small effects on the frictional wind components.

### 5.2.3 Vertical wind profile

To further investigate the effects of the rain field on the vertical wind profile within the tropical cyclone boundary layer, a case study is presented in Fig 12.

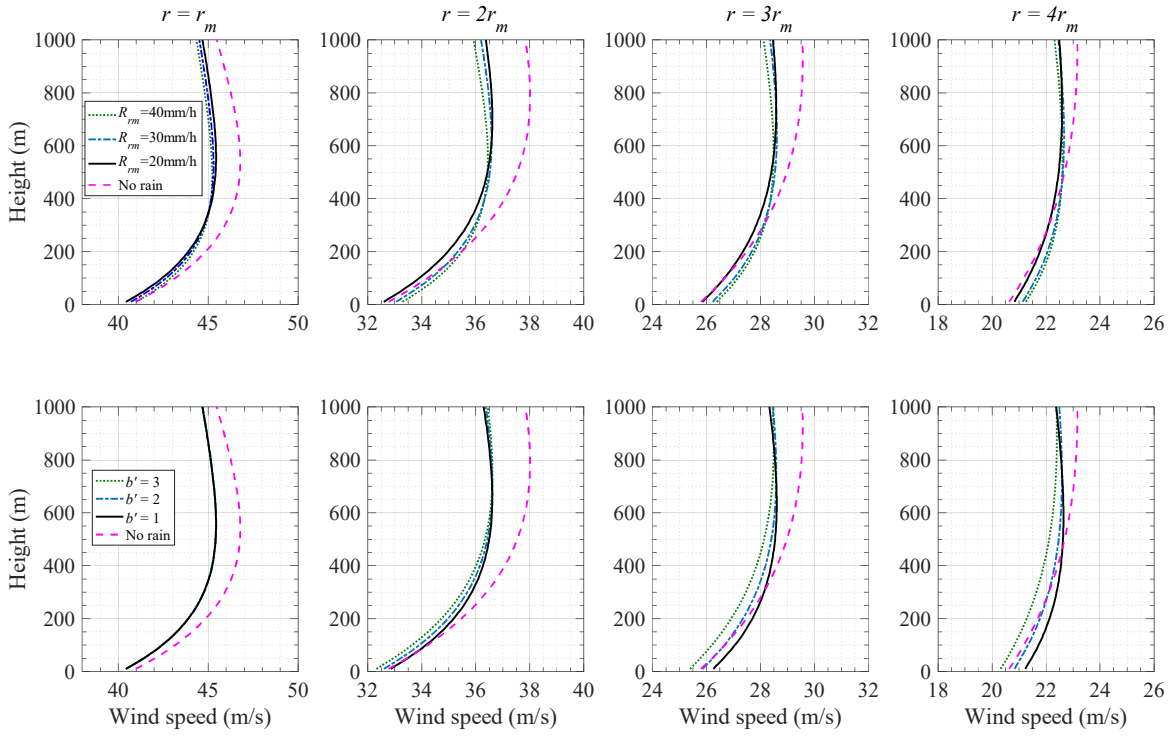


**Fig. 12.** Sensitivity analysis of the vertical wind profile at four different radial locations with $\theta = 0°$

As discussed in Sect. 4, the rain-induced effects on the wind profiles are mainly governed by the transfer of momentum between the wind and raindrops. The wind speed increases downward until reaching the supergradient region. Accordingly, the wind speed is decelerated by imparting momentum to the raindrops, as presented in Fig. 12. It is noted that the height $\delta$ of supergradient wind at the location of maximum winds (i.e., $r = r_m$) is equal to 470m for $R_{rm} = 40mm/h$, 520m for $R_{rm} = 30mm/h$, 540m for $R_{rm} = 20mm/h$, and 560m for $R_{rm} = 0$. This observation indicates that the precipitation may lead to a decrease of the supergradient wind height (e.g., Zhang et al. 2011).

393 Below the supergradient region the mean wind speed decreases downward, and the speed of
394 raindrops, due to their inertia, is generally larger than the corresponding wind speed (Choi 2001;
395 Fu et al. 2015). As a result, the raindrops impart momentum to the wind and hence accelerate its
396 speed. However, the amount of momentum transferred from the raindrops to the wind below the
397 supergradient region may not be sufficient to significantly modify the vertical wind profiles, as
398 shown in Fig. 12. The simulation results of rain-induced effects on surface winds are similar to the
399 findings of several previous studies (e.g., Caldwell and Elliott 1971; 1972).

400 It is noted that the Fig. 12 is based on marine condition. For the landfall scenarios, the
401 surface roughness is expected to increase significantly. Accordingly, the supergradient wind region
402 will be modified (e.g., increase of height) and hence the momentum exchange mechanism between
403 the wind and rain particles may change. Since the storm intensity was not involved in the
404 development of the proposed analysis framework to consider rain-induced effects on tropical-
405 cyclone boundary-layer winds, the same methodology used for estimating the results in Fig. 12
406 could be employed to obtain the simulation results for storms of other intensities.

407 **5.2.4 Discussions**

408 The major purpose of this study is to develop an analysis framework to consider the rain-induced
409 effects on the tropical-cyclone boundary-layer winds. As shown in previous sections, the rainfall
410 may present considerable effects on both wind speed and direction. While the wind speed can be
411 either accelerated or decelerated, the wind direction (and hence inflow angle) might significantly
412 change. Both wind speed and direction will modify the wind loading on buildings and other
413 structures in coastline areas (e.g., Huang and Xu 2011; Huang et al. 2011; Huang and Xu 2012).
414 The developed analysis framework of tropical-cyclone boundary-layer winds, due to its high
415 computational efficiency, can be used in conjunction with the Monte Carlo techniques to perform
416 risk analysis of tropical-cyclone wind hazards. In addition, it can be employed to estimate the

417 design wind speed and its direction at the desired locations for a given return period based on
418 hurricane tracking approach (Vickery et al. 2000). Accordingly, the obtained directional design
419 wind speed actually integrates the important contributions from the tropical-cyclone rainfall.
420 Hence, the design wind loads for building and other structures in the hurricane-prone areas would
421 be changed by consideration of rain-induced effects on wind field. It should be noted that the
422 contribution from the rain impacts towards the total loading is trivial (e.g., Bitsuamlak et al. 2009;
423 Baheru 2014; Johnson et al. 2018). Actually, the rain is primarily responsible for damage to interior
424 contents (e.g., Johnson et al. 2018). Specifically, raindrops impinge on the building envelope and
425 penetrate the façade through defects (e.g., resulting from wind-borne debris impact, excessive
426 internal/external pressures, and excessive structural response). The simplification of the fully-
427 coupled dynamic system governing the raindrop motion and the wind field to a weakly-coupled
428 one represented by aerodynamic drag force actually results in a first-order approximation of the
429 wind-rain interactions. It is noted that the first-order approximation in terms of drag coefficient is
430 popularly used in the transfer of horizontal momentum between air and rain (e.g., Caldwell and
431 Elliott 1971; 1972) and between air and land/ocean (e.g., Meng et al. 1995; Kepert 2001; Huang
432 and Xu 2012). Accordingly, the nonlinear effects resulting from the higher-order terms in the
433 wind-rain interactions are ignored. More comprehensive validation of the developed analysis
434 framework to consider the rain-induced effects on the tropical-cyclone boundary-layer winds
435 should be carried out in the future based on the wind tunnel testing that is equipped with rain
436 simulation capabilities.

437 **Concluding Remarks**

438 The rain-induced effects on the boundary-layer wind field of tropical cyclones were investigated
439 in this study. The fully-coupled dynamic system governing the wind and raindrops fields was
440 simplified into a weakly-coupled one represented by aerodynamic drag force. The drag-induced

441 horizontal momentum transfer was integrated into the governing equations of the linear, height-
442 resolving wind field, and an analytical model was accordingly developed to effectively consider
443 the rain-induced effects on the boundary-layer winds of tropical cyclones. It is noted that the rain
444 rate *R*, correlation parameter $\gamma$ , drag coefficient $C_r$ and raindrop size *d* are essential factors in the
445 consideration of rain-induced effects on boundary-layer winds. While the values of $\gamma$ and $C_r$ are
446 easily obtained from the literature, two parametric rain rate profiles corresponding to the marine
447 and landfalling conditions were developed here. In addition, the three-parameter gamma model for
448 the raindrop size distribution was used in this study to randomly generate the raindrop sizes in the
449 simulation of the wind speed components using the Monte Carlo technique. Sensitivity analyses
450 were performed to assess the contribution of the essential rain parameters to the modification of
451 wind field. In general, the raindrop drag coefficient $C_r$ has relative small effects on the boundary-
452 layer winds. Although the wind speed can be either accelerated or decelerated depending on the
453 location in the tropical cyclones (i.e., eyewall and outer vortex regions) and the rain parameters,
454 the rain-induced effects on the wind speeds in the upper region of the boundary layer (i.e., above
455 the supergradient region) are more considerable compared to those in the lower region.
456 Furthermore, it has been demonstrated that the rain-induced effects on the boundary-layer wind
457 directions (and hence the inflow angle) are significant in the tropical cyclone eyewall region. This
458 observation may have important implications to the tropical cyclone wind hazard on tall buildings
459 and other structures.

460 **Acknowledgments**

461 The support for this project provided by the NSF Grant # CMMI 15-37431 is gratefully
462 acknowledged.

463 **References**

Aylor, D.E. and Ducharme, K.M., 1995. Wind fluctuations near the ground during rain. Agricultural and forest meteorology, 76(1), pp.59-73.

Baheru, T., Chowdhury, A.G., Bitsuamlak, G., Masters, F.J. and Tokay, A., 2014. Simulation of wind-driven rain associated with tropical storms and hurricanes using the 12-fan Wall of Wind. Building and Environment, 76, pp.18-29.

Baheru, T., 2014. Development of test-based wind-driven rain intrusion model for hurricane-induced building interior and contents damage. PhD Thesis Florida International University, Florida, USA.

Best, A.C., 1950. The size distribution of raindrops. Quarterly Journal of the Royal Meteorological Society, 76(327), pp.16-36.

Bitsuamlak, G.T., Chowdhury, A.G. and Sambare, D., 2009. Application of a full-scale testing facility for assessing wind-driven-rain intrusion. Building and Environment, 44(12), pp.2430-2441.

Blocken, B. and Carmeliet, J., 2000a. Driving rain on building envelopes-I. Numerical estimation and full-scale experimental verification. Journal of Thermal Envelope and Building Science, 24(1), pp.61-85.

Blocken, B. and Carmeliet, J., 2000b. Driving rain on building envelopes—II. Representative experimental data for driving rain estimation. Journal of Thermal Envelope and Building Science, 24(2), pp.89-110.

Blocken, B. and Carmeliet, J., 2004. A review of wind-driven rain research in building science. Journal of wind engineering and industrial aerodynamics, 92(13), pp.1079-1130.

Caldwell, D.R. and Elliott, W.P., 1971. Surface stresses produced by rainfall. Journal of Physical Oceanography, 1(2), pp.145-148.

Caldwell, D.R. and Elliott, W.P., 1972. The effect of rainfall on the wind in the surface layer. Boundary-Layer Meteorology, 3(2), pp.146-151.

Choi, E.C., 2001. Wind-driven rain and driving rain coefficient during thunderstorms and non-thunderstorms. Journal of wind engineering and industrial aerodynamics, 89(3), pp.293-308.

Fu, X., Li, H.N. and Yi, T.H., 2015. Research on motion of wind-driven rain and rain load acting on transmission tower. Journal of Wind Engineering and Industrial Aerodynamics, 139, pp.27-36.

Gunn, R. and Kinzer, G.D., 1949. The terminal velocity of fall for water droplets in stagnant air. Journal of Meteorology, 6(4), pp.243-248.

Georgiou, P.N., 1986. Design wind speeds in tropical cyclone-prone regions. PhD Thesis University of Western Ontario, London, Ontario, Canada.

Guo, J.C., Urbonas, B. and Stewart, K., 2001. Rain catch under wind and vegetal cover effects. Journal of Hydrologic Engineering, 6(1), pp.29-33.

Harrison, E.L., Veron, F., Ho, D.T., Reid, M.C., Orton, P. and McGillis, W.R., 2012. Nonlinear interaction between rain-and wind-induced air-water gas exchange. Journal of Geophysical Research: Oceans, 117(C3).

Ho, D.T., Veron, F., Harrison, E., Bliven, L.F., Scott, N. and McGillis, W.R., 2007. The combined effect of rain and wind on air–water gas exchange: A feasibility study. Journal of Marine Systems, 66(1), pp.150-160.

Holland, G.J., 1980. An analytic model of the wind and pressure profiles in hurricanes. Monthly weather review, 108(8), pp.1212-1218.

Huang, S.H. and Li, Q.S., 2010. Numerical simulations of wind-driven rain on building envelopes based on Eulerian multiphase model. Journal of Wind Engineering and Industrial Aerodynamics, 98(12), pp.843-857.

Huang, W.F. and Xu, Y.L., 2011. Numerical models for simulating typhoon wind fields in boundary layer. Proceedings of the 8th International Advanced School in Wind Engineering, November, Hong Kong, pp.1-17.

506 Huang, W.F., Xu, Y.L., Li, C.W. and Liu, H.J., 2011. Directional typhoon wind speeds and profiles in Hong Kong.
507 Proceedings of the 8th International Advanced School in Wind Engineering, November, Hong Kong, pp.18-
508 33.

509 Huang, W.F. and Xu, Y.L., 2012. A refined model for typhoon wind field simulation in boundary layer. Advances in
510 Structural Engineering, 15(1), pp.77-89.

511 Jakobsen, F. and Madsen, H., 2004. Comparison and further development of parametric tropical cyclone models for
512 storm surge modelling. Journal of Wind Engineering and Industrial Aerodynamics, 92(5), pp.375-391.

513 Janin, L.F. and Cermak, J.E., 1988. Sediment-laden velocity profiles developed in a long boundary-layer wind tunnel.
514 Journal of Wind Engineering and Industrial Aerodynamics, 28(1-3), pp.159-168.

515 Jarvinen, B.R., Neumann, C.J. and Davis, M.A.S., 1984. A tropical cyclone data tape for the North Atlantic Basin,
516 1886–1983: Contents, limitations. and uses. Tech. Memo. NWS NHC 22, National Oceanic and Atmospheric
517 Administration.

518 Johnson, T., Pinelli, J.P., Baheru, T., Chowdhury, A.G., Weekes, J. and Gurley, K., 2018. Simulation of Rain
519 Penetration and Associated Damage in Buildings within a Hurricane Vulnerability Model. Natural Hazards
520 Review, 19(2), p.04018004.

521 Kepert, J., 2001. The dynamics of boundary layer jets within the tropical cyclone core. Part I: Linear theory. Journal
522 of the Atmospheric Sciences, 58(17), pp.2469-2484.

523 Landsea, C.W., 2000. Climate variability of tropical cyclones: past, present and future. Storms. Routledge, New York,
524 pp.220-241.

525 Langousis, A. and Veneziano, D., 2009. Theoretical model of rainfall in tropical cyclones for the assessment of long-
526 term risk. Journal of Geophysical Research: Atmospheres, 114(D2).

527 Liggett, J.A., 1994. Fluid Mechanics–McGraw-Hill. New York.

528 Lopez, C.R., 2011. Measurement, analysis, and simulation of wind driven rain. PhD Thesis University of Florida, ,
529 Florida, USA.

530 Lonfat, M., Marks Jr, F.D. and Chen, S.S., 2004. Precipitation distribution in tropical cyclones using the Tropical
531 Rainfall Measuring Mission (TRMM) microwave imager: A global perspective. Monthly Weather
532 Review, 132(7), pp.1645-1660.

533 Marshall, J.S. and Palmer, W.M.K., 1948. The distribution of raindrops with size. J. Meteor., 5, pp.165-166.

534 Meng, Y., Matsui, M. and Hibi, K., 1995. An analytical model for simulation of the wind field in a typhoon boundary
535 layer. Journal of Wind Engineering and Industrial Aerodynamics, 56(2-3), pp.291-310.

536 Myers, V.A. and Malkin, W., 1961. Some properties of hurricane wind fields as deduced from trajectories. US
537 Department of Commerce, Weather Bureau.

538 Niu, H., Dong, G., Ma, X. and Ma, Y., 2016. An analytical model of a typhoon wind field based on spiral trajectory.
539 Proceedings of the Institution of Mechanical Engineers, Part M: Journal of Engineering for the Maritime
540 Environment, p.1475090216682881.

541 Okaruma, S. and Nakanishi, K., 1969. Theoretical study on sprinkler sprays (part four) geometric pattern form of
542 single sprayer under wind conditions. Trans. Jpn. Soc. Irrig. Drain. Reclam. Eng, 29, pp.35-43.

543 Pauluis, O. and Dias, J., 2012. Satellite estimates of precipitation-induced dissipation in the atmosphere. Science,
544 335(6071), pp.953-956.

545 Pielke, R.A. and Lee, T.J., 1991. Influence of sea spray and rainfall on the surface wind profile during conditions of
546 strong winds. Boundary-Layer Meteorology, 55(3), pp.305-308.

Poreh, M. and Mechrez, E., 1984. The combined effect of wind and topography on rainfall distribution. Journal of Hydrology, 72(1-2), pp.1-23.

Rappaport, E.N., 2000. Loss of life in the United States associated with recent Atlantic tropical cyclones. Bulletin of the American Meteorological Society, 81(9), pp.2065-2073.

Sabuwala, T., Gioia, G. and Chakraborty, P., 2015. Effect of rainpower on hurricane intensity. Geophysical Research Letters, 42(8), pp.3024-3029.

Shapiro, A., 2005. Drag-induced transfer of horizontal momentum between air and raindrops. Journal of the atmospheric sciences, 62(7), pp.2205-2219.

Snaiki, R. and Wu, T., 2017a. A linear height-resolving wind field model for tropical cyclone boundary layer. Journal of Wind Engineering and Industrial Aerodynamics, 171, pp.248-260.

Snaiki, R. and Wu, T., 2017b. Modeling tropical cyclone boundary layer: Height-resolving pressure and wind fields. Journal of Wind Engineering and Industrial Aerodynamics, 170, pp.18-27.

Snaiki, R. and Wu, T., 2018a. A semi-empirical model for mean wind velocity profile of landfalling hurricane boundary layers. Journal of Wind Engineering and Industrial Aerodynamics, 180, pp.249-261.

Snaiki, R. and Wu, T., 2018b. An analytical framework for rapid estimate of rain rate during tropical cyclones. Journal of Wind Engineering and Industrial Aerodynamics, 174, pp.50-60.

Testud, J., Oury, S., Black, R.A., Amayenc, P. and Dou, X., 2001. The concept of "normalized" distribution to describe raindrop spectra: A tool for cloud physics and cloud remote sensing. Journal of Applied Meteorology, 40(6), pp.1118-1140.

Tokay, A. and Short, D.A., 1996. Evidence from tropical raindrop spectra of the origin of rain from stratiform versus convective clouds. Journal of applied meteorology, 35(3), pp.355-371.

Tokay, A., Bashor, P.G., Habib, E. and Kasparis, T., 2008. Raindrop size distribution measurements in tropical cyclones. Monthly Weather Review, 136(5), pp.1669-1685.

Tuleya, R.E., DeMaria, M. and Kuligowski, R.J., 2007. Evaluation of GFDL and simple statistical model rainfall forecasts for US landfalling tropical storms. Weather and forecasting, 22(1), pp.56-70.

Ulbrich, C.W., 1983. Natural variations in the analytical form of the raindrop size distribution. Journal of climate and applied meteorology, 22(10), pp.1764-1775.

Vickery, P.J., Skerlj, P.F. and Twisdale, L.A., 2000. Simulation of hurricane risk in the US using empirical track model. Journal of structural engineering, 126(10), pp.1222-1237.

Vogl, S. and Smith, R.K., 2009. Limitations of a linear model for the hurricane boundary layer. Quarterly Journal of the Royal Meteorological Society, 135(641), pp.839-850.

Willis, P.T., 1984. Functional fits to some observed drop size distributions and parameterization of rain. Journal of the atmospheric sciences, 41(9), pp.1648-1661.

Willis, P.T. and Tattelman, P., 1989. Drop-size distributions associated with intense rainfall. Journal of applied meteorology, 28(1), pp.3-15.

Willoughby, H.E., Darling, R.W.R. and Rahn, M.E., 2006. Parametric representation of the primary hurricane vortex. Part II: A new family of sectionally continuous profiles. Monthly weather review, 134(4), pp.1102-1120.

Yurchak, B.S., 2007. Description of cloud-rain bands in a tropical cyclone by a hyperbolic-logarithmic spiral. Russian Meteorology and Hydrology, 32(1), pp.8-18.

Zhang, J.A., Rogers, R.F., Nolan, D.S. and Marks Jr, F.D., 2011. On the characteristic height scales of the hurricane boundary layer. Monthly Weather Review, 139(8), pp.2523-2535.